



Short communication

Nanoporous gold on three-dimensional nickel foam: An efficient hybrid electrode for hydrogen peroxide electroreduction in acid media

Xi Ke ^a, Yantong Xu ^a, Changchun Yu ^b, Jie Zhao ^b, Guofeng Cui ^{a,*}, Drew Higgins ^c, Qing Li ^c, Gang Wu ^{c,d}

^a Electronic Packaging Electrochemistry Laboratory, School of Chemistry and Chemical Engineering, Sun Yat-sen University, Guangzhou 510275, China

^b School of Mechanical and Automotive Engineering, South China University of Technology, Guangzhou 510640, China

^c Materials Physics and Applications Division, Los Alamos National Laboratory, Los Alamos, NM 87545, United States

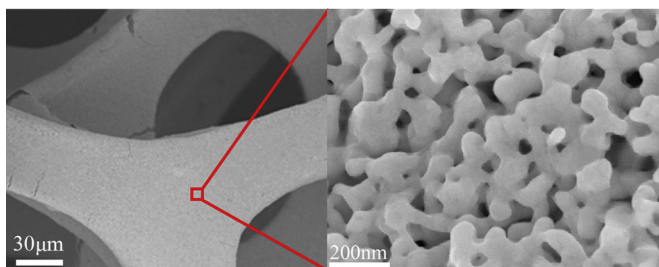
^d Department of Chemical and Biological Engineering, University at Buffalo, The State University of New York, Buffalo, NY 14260, United States



HIGHLIGHTS

- A novel method to fabricate nanoporous gold (NPG) by chemical dealloying of electrodeposited Au–Sn alloy.
- NPG was produced on three dimensional (3D) Ni foam surface.
- The good electrochemical performance is achieved on the 3D NPG/Ni foam hybrid electrode.
- The 3D NPG/Ni foam hybrid electrode exhibits superior activity and excellent durability toward H₂O₂ electroreduction.

GRAPHICAL ABSTRACT



ARTICLE INFO

Article history:

Received 12 May 2014

Received in revised form

2 July 2014

Accepted 2 July 2014

Available online 10 July 2014

Keywords:

Electrodes

Nanoporous gold

Nickel foam

Hydrogen peroxide electroreduction

Porous materials

ABSTRACT

A hybrid structure of nanoporous gold (NPG) on three-dimensional (3D) macroporous Ni foam has been synthesized by electrodeposition of Au–Sn alloy film followed by a facile chemical dealloying process under free corrosion conditions. Scanning electron microscopy (SEM) and X-ray diffraction (XRD) are used to characterize the morphology and structure of the NPG/Ni foam hybrids. It is shown that the Ni foam skeletons are uniformly wrapped by the NPG film which is composed of bicontinuous nanostructures consisting of interconnected ligaments and nanopores. Electroreduction of H₂O₂ on the NPG/Ni foam hybrid electrode in acid media is investigated by linear scan voltammetry, chronoamperometry and electrochemical impedance spectroscopy. It is found that such hierarchical porous electrode displays superior activity, durability and mass transport property for H₂O₂ electroreduction. These results demonstrate the potential of the NPG/Ni foam hybrid electrodes for the applications in fuel cell technology.

© 2014 Elsevier B.V. All rights reserved.

1. Introduction

Hydrogen peroxide (H₂O₂) has been extensively investigated as the oxidizer to replace oxygen for some types of fuel cells, such as

direct borohydride-hydrogen peroxide fuel cells [1–3] and direct hydrazine-hydrogen peroxide fuel cells [4,5]. These particular chemistries are best suited for air-independent applications under extreme conditions such as outer space and underwater environments. Compared to oxygen, H₂O₂ as the oxidizer allows much improved reaction kinetics on the cathode together with higher power densities and theoretical open circuit voltages [2,6].

* Corresponding author.

E-mail addresses: cuigf@mecart.cn, cuigf@mail.sysu.edu.cn (G. Cui).

Designing cathode catalysts with improved H₂O₂ reduction kinetics can furthermore improve the performance of these fuel cell technologies [7,8], and a variety of different catalyst materials have been investigated including noble metals [9,10] and transition metal oxides [11,12]. Among these, nanostructured gold-based catalysts, such as nanoparticles [13,14], clusters [15] and nanodendrites [16] have drawn great attention due to their high chemical stability and excellent electrocatalytic performance toward H₂O₂ reduction. However, the current gold nanostructure-based electrodes suffer from several disadvantages including non-uniform dispersion, structural discontinuity and severe agglomeration during operation. Therefore, there remains great demand to pursue alternative nanostructure control strategies to design electrodes with improved utilization and efficiency toward H₂O₂ electroreduction.

Recently, nanoporous gold (NPG) materials have stimulated great research interest due to their intriguing properties [17–21] that arise from their unique bicontinuous structure consisting of both solid ligaments and void channels. The excellent structural integrity, mechanical stability, chemical stability and electrical conductivity of NPG has been demonstrated beneficial for a variety of different applications including heterogeneous catalysis [22–24], surface enhanced Raman scattering (SERS) [25,26], supercapacitors [27,28], electrochemical actuators [29] and biosensors [30]. NPG electrodes have also been successfully developed for the electrochemical reduction of H₂O₂ [31], accomplished using thin, two-dimensional (2D) planar electrode structures. In order to improve the efficiency of these electrodes, it is however important to increase the catalyst surface area that is available to facilitate the H₂O₂ electroreduction. In this context, the development of interconnected, three-dimensional (3D) NPG electrode structures would therefore provide significant improvements.

In the present work, NPG supported on 3D Ni foam are prepared as unique electrode structure for H₂O₂ electroreduction. The preparation process involves electrodeposition of an Au–Sn alloy film on the surface of the Ni foam, followed by a chemical dealloying process in which the tin component is etched away. The 3D Ni foam is a low cost metal substrate with high surface area and high conductivity, which has been applied as a template to host catalysts for effectively increasing the number of reaction sites [32–34]. There have been several reports that demonstrated successful synthesis of H₂O₂ electroreduction catalysts on the Ni foam skeleton [11,12,14]. However, in all of these studies, electrochemical reduction of H₂O₂ was conducted in alkaline media, probably because the Ni foam substrate is not suitable for use in electroreduction of H₂O₂ in acid solutions due to its instability. Nevertheless, the decomposition of H₂O₂ exhibits fast kinetics in alkaline media than that in acid media, which decreases the utilization efficiency of H₂O₂ [35]. In this context, it is considered to be a challenge to grow nanostructures on the Ni foam support as the electrocatalyst for H₂O₂ reduction in acid media. Herein, we demonstrate that the NPG film grown on Ni foams not only efficiently increases their stability in acid media, but also exhibits high catalytic activity toward H₂O₂ electroreduction in acid media. To the best of our knowledge, this is the first time that the Ni foam supported catalyst is developed for H₂O₂ electroreduction in acid media. It is believed that the NPG/Ni foam hybrid electrode with 3D hierarchical porous structures demonstrated in the present work will be a promising type of electrode material for the applications in a broad range of electrochemical processes.

2. Experimental

2.1. Electrode fabrication

The NPG/Ni foam hybrid electrode was prepared by a facile two-step procedure. First, the Au–Sn alloy film was grown on Ni

foam by an electrodeposition process. In detail, Ni foam (20 mm × 60 mm × 0.1 mm, 100 pores per inch, 330 g m⁻², Changsha Lyrun Material Co., Ltd., China) was pretreated with 5 M HCl solution for 30 min to remove any potential nickel oxide species on the surface, and then rinsed with deionized water. An Au–Sn alloy film was deposited onto the pretreated Ni foam by a cathodic electrodeposition method using a constant current of 5 mA cm⁻² for 5 min at 45 °C, operated by a KR-3001 30V/1A programmable DC sourcemeter (Kingrang Electronic Technology Co., Ltd., Shenzhen, China) and an Au–Sn alloy plating solution (Huizhou Leadao Electronic Material Co., Ltd., Huizhou, China. Website: www.leadao.cn). After deposition, the as-prepared Au–Sn alloy/Ni foam electrode was rinsed with deionized water and dried in air. In the second step, the Ni foam coated with an Au–Sn alloy film was immersed into 5 M NaOH and 1 M H₂O₂ solution at room temperature for 3 days. After free corrosion, the substrates were thoroughly rinsed with deionized water and dried in air.

2.2. Characterization

The morphology was examined using a field-emission scanning electron microscopy (SEM, JEOL, JSM-6700F, 15 keV). The crystal structure was analyzed by x-ray diffraction (XRD, Rigaku D/max-2200/PC) using Cu K α radiation. Cyclic voltammetry (CV), linear scan voltammetry (LSV), chronoamperometry (CA) and electrochemical impedance spectroscopy (EIS) experiments (Gamry REF 600 Electrochemical Workstation) were performed in a conventional three-electrode electrochemical cell at room temperature using 0.5 M H₂SO₄ as the electrolyte. The Ni foam supported NPG (~4 cm² area) acted as the working electrode. A platinum plate and saturated calomel electrode (SCE) were used as the counter electrode and the reference electrode, respectively. EIS measurements were conducted by applying an AC voltage with 5 mV amplitude in a frequency range from 0.01 to 100 kHz.

3. Results and discussion

SEM images for the as-obtained Ni foam substrate at various magnifications are shown in Fig. 1A–C, displaying a 3D, highly porous and cross-linked structure. The average pore size of the Ni foam is about 100–200 μm, and the Ni grains of the skeleton can be seen at a higher magnifications (Fig. 1B and C). Fig. 1D–F displays the SEM images after the Au–Sn alloy film was deposited on the pretreated Ni foam using a cathodic electrodeposition method. It can be seen that the Ni foam surfaces are completely covered with small grains with an average size of 150 nm. After chemical dealloying of the Au–Sn alloy film, SEM images of the NPG film completely covering the surface of the Ni foam are shown in Fig. 1G–I. Comparing Fig. 1C with Fig. 1I, it is easily seen that the electrodeposition process followed by chemical dealloying of the Au–Sn alloy film results in a significant morphology change of the Ni foam surface, demonstrating the efficient formation of an NPG film. The high resolution SEM image (Fig. 1J) reveals that the film is composed of sponge-like bicontinuous nanostructures, which consist of interconnected ligaments and nanopores. The ligament size is about 50–100 nm and the pore size is 30–90 nm. The amount of Au on the Ni foam can be calculated from the mass difference between the bare Ni foam and the NPG-coated Ni foam. Therefore, the Au loading on the Ni foam is determined to be 150 μg cm⁻².

The crystal phase of the samples was examined by XRD, whereby the bare Ni foam shows three diffraction peaks at $2\theta = 44.3^\circ$, 51.8° and 76.2° (Fig. 2, black line). These peaks can be indexed to the (111), (200) and (220) planes of the face centered

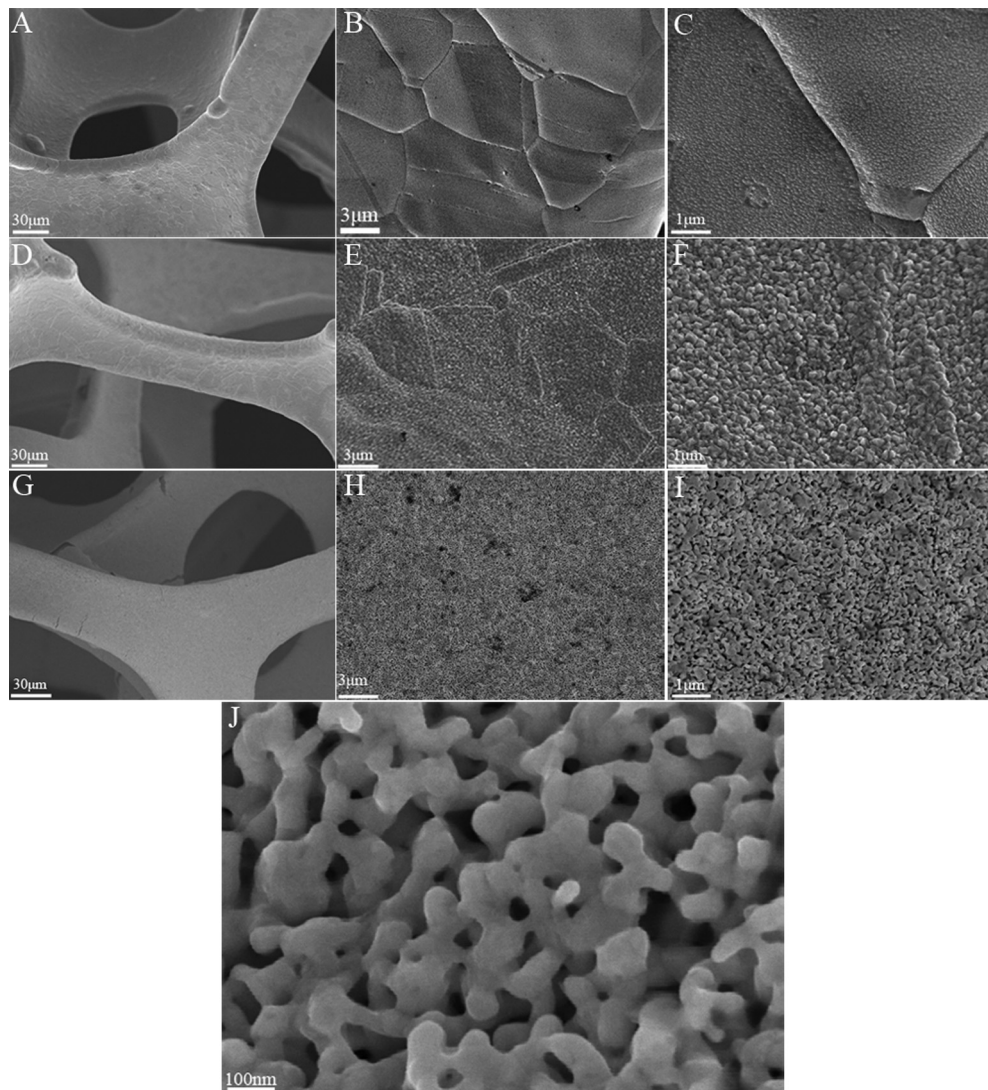


Fig. 1. SEM images of the as-obtained Ni foam at different magnifications (A, B, C), SEM images with different magnification of the Ni foam surfaces after Au–Sn alloy film was electrodeposited (D, E, F) and SEM images with different magnifications of the Ni foam surfaces after chemical dealloying of electrodeposited Au–Sn alloy film (G, H, I). High resolution SEM image (J) of the sample in shown in (I).

cubic (fcc) phase Ni (JCPDS File No. 04-0850), respectively. After the electrodeposition and subsequent dealloying process, new diffraction peaks appearing in the XRD pattern of the NPG on Ni foam ([Fig. 2](#), red line (in the web version)) at $2\theta = 38.1^\circ, 64.6^\circ, 77.5^\circ$

and 81.5° can be well indexed to the (111), (220), (311) and (222) planes of fcc Au (JCPDS File No. 04-0784), respectively. It should be noted that the cubic Ni(111) peak almost overlaps with cubic Au(200) peak. The above XRD results demonstrate that the less noble component (Sn) of the Au–Sn alloy is completely leached out during the dealloying process.

The electrochemical performance of the unique NPG/Ni foam hybrid electrodes toward H_2O_2 electroreduction in acidic media was evaluated using several electrochemical techniques. The inset in [Fig. 3](#) gives the representative CV curve of the NPG/Ni foam hybrid electrode in a 0.5 mol L^{-1} H_2SO_4 solution at a scan rate of 50 mV s^{-1} . The shape of the CV curve is in conformity with the typical electrochemical signature of a polycrystalline Au electrode in acidic solutions, in other words, the anodic peak and cathodic peak represent the formation and reduction of surface gold oxide species, respectively [31]. Furthermore, the fact that no irregular peaks exist besides the Au oxidation and reduction peaks supplies additional evidence that Sn is fully etched away from the Au–Sn alloy. The hierarchical porous structure leads to a substantial increase of the effective surface area. The electrochemical active surface area (ECSA) of the NPG/Ni foam hybrid electrode was determined by integrating the peak area corresponding to Au oxide

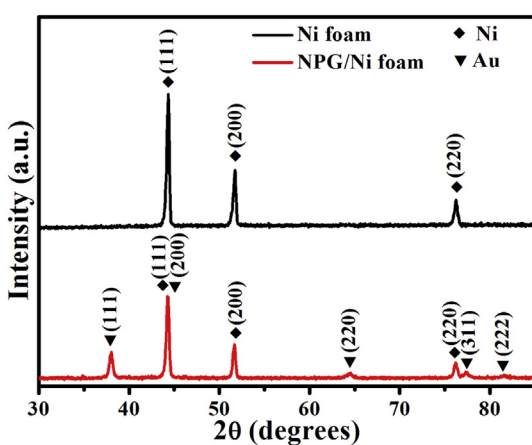


Fig. 2. XRD patterns of as-obtained Ni foam and the NPG/Ni foam hybrid electrode.

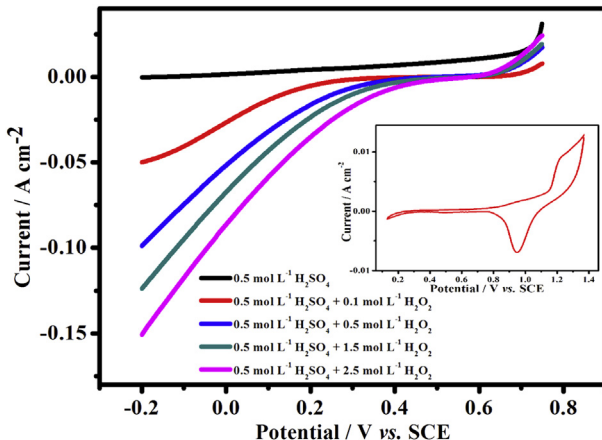


Fig. 3. Linear scan voltammetric curves for H_2O_2 electroreduction at various H_2O_2 concentrations on the NPG/Ni foam hybrid electrode. Electrolyte: $0.5 \text{ mol L}^{-1} + \text{H}_2\text{O}_2$. Scan rate: 5 mV s^{-1} . Inset: cyclic voltammogram for the NPG/Ni foam hybrid electrode in a $0.5 \text{ mol L}^{-1} \text{H}_2\text{SO}_4$ solution at a scan rate of 50 mV s^{-1} . The current was normalized by the geometrical area of the Ni foam.

reduction. Based on a value of $390 \mu\text{C cm}^{-2}$ used for polycrystalline Au electrode [36], The ECSA for the NPG/Ni foam hybrid electrode was $32.1 \text{ m}^2 \text{ g}^{-1}$, which implies a surface roughness factor of ~ 48 . These results prove that the micro/nanoporous structure effectively increases the real surface area. It is worth noting that the bare Ni foam electrode dissolves rapidly in the $0.5 \text{ mol L}^{-1} \text{H}_2\text{SO}_4$ solution, while the NPG/Ni foam hybrid electrode remains stable throughout the entire period of the experiment (data not shown). Thus it is suggested that the NPG film is able to protect the Ni foam from oxidative corrosion in this acidic environment. Fig. 3 shows the polarization curves (measured current normalized by the geometrical area of the Ni foam) for H_2O_2 electroreduction at various H_2O_2 concentrations on the NPG/Ni foam hybrid electrode. It can be observed that the onset reduction potential is ca. 0.6 V vs SCE and independent of the H_2O_2 concentration. The current densities increase with the increase of H_2O_2 concentration, but the rate of increase slowed down with higher H_2O_2 amounts due to the significant decomposition of H_2O_2 at high concentrations.

The durability of the NPG/Ni foam hybrid electrode for H_2O_2 electroreduction was examined by chronoamperometric measurements. Fig. 4 displays chronoamperometric curves of H_2O_2 electroreduction in $0.5 \text{ mol L}^{-1} \text{H}_2\text{SO}_4 + 1.5 \text{ mol L}^{-1} \text{H}_2\text{O}_2$ on the NPG/Ni foam hybrid electrode. The potentials were chosen in the range according to the polarization curves in Fig. 3. It is observed that the reduction currents reach steady-state immediately after a constant potential is applied. The current density is nearly constant at more positive electrode potentials (e.g., 0.35 V), demonstrating that the NPG/Ni foam hybrid electrode exhibits a superior durability for H_2O_2 electroreduction. However, the reduction currents slightly decreased during the measurements at more negative electrode potentials (e.g., 0.15 V and 0.05 V), which is probably due to a decrease of H_2O_2 concentration at the electrode surface resulting from the continued consumption of H_2O_2 during the chronoamperometric measurements. These results are also in good agreement with previous reports [37,38].

Moreover, the CA curves for H_2O_2 electroreduction at the different potentials were tested by using the same electrode, namely the NPG/Ni foam hybrid electrode was examined for 6400 s. These results demonstrate that the NPG/Ni foam hybrid electrode exhibits excellent durability for catalyzing H_2O_2 electroreduction. Fig. 5 shows the EIS spectra of the NPG/Ni foam electrode tested at different potentials in H_2SO_4 solution with and without H_2O_2 . In the absence of H_2O_2 , the spectrum displays a straight line (Fig. 5,

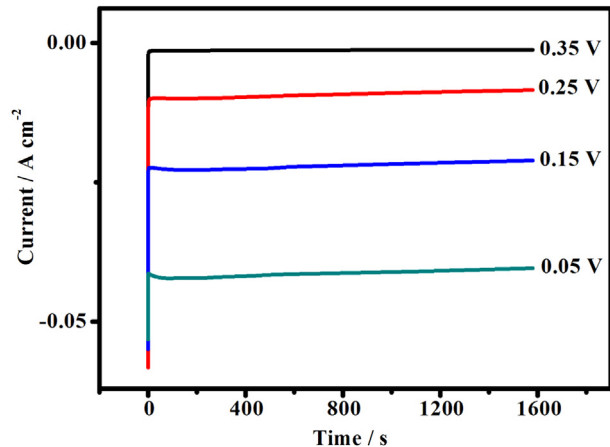


Fig. 4. Chronoamperometric curves for H_2O_2 electroreduction on the NPG/Ni foam hybrid electrode. Electrolyte: $0.5 \text{ mol L}^{-1} \text{H}_2\text{SO}_4 + 1.5 \text{ mol L}^{-1} \text{H}_2\text{O}_2$.

bottom inset). In the presence of H_2O_2 , the spectra at all potentials show a semicircle spanning the high and low frequency regions. The diameter of this semicircle becomes smaller as the electrode potential becoming more negative. This suggesting that the semicircle size most probably corresponds to the H_2O_2 electroreduction, because the semicircles appear only in the presence of H_2O_2 and the H_2O_2 electroreduction rate is electrode potential dependent. In other words, the more negative the electrode potential, the faster the reaction rate (Fig. 4) and the smaller the diameter of the semicircle (Fig. 5). The experimental data are simulated using an equivalent circuit composed of a constant phase element (CPE)/resistive element and a resistance in series (Fig. 5, top left inset). The simulation results (solid line) fitted well with the experimental data (symbols). R is the ohmic resistance of the electrode and electrolyte. R_1 is the charge transfer resistance of the H_2O_2 electroreduction. Q is the corresponding constant phase angle element. According to the simulation, the value of R is around $2.7 \Omega \text{ cm}^2$ and is independent of the electrode potentials. The value of R_1 decreased with the negative shift of the potentials from $60.3 \Omega \text{ cm}^2$ (0.35 V) to $14.3 \Omega \text{ cm}^2$ (0.25 V), $4.4 \Omega \text{ cm}^2$ (0.15 V) and $2.0 \Omega \text{ cm}^2$

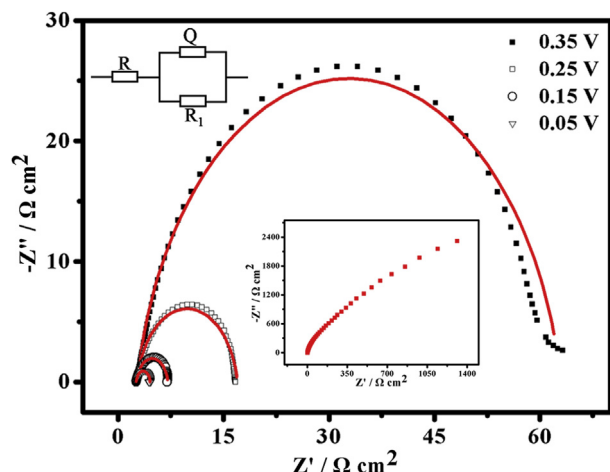


Fig. 5. Electrochemical impedance spectra (EIS) of the NPG/Ni foam hybrid electrode, measured at different potentials in the electrolyte of $0.5 \text{ mol L}^{-1} \text{H}_2\text{SO}_4 + 1.5 \text{ mol L}^{-1} \text{H}_2\text{O}_2$. Scattered symbols: experimental data. Solid lines: simulated results. The bottom inset is the EIS spectrum of the NPG/Ni foam hybrid electrode measured at 0.35 V in a $0.5 \text{ mol L}^{-1} \text{H}_2\text{SO}_4$ solution. The top left inset is the equivalent circuit employed to simulate the experimental results.

(0.05 V), indicating that the H₂O₂ electroreduction is faster at more negative potentials, which is in agreement with the results depicted in Fig. 4.

4. Conclusions

In summary, NPG films were successfully formed on 3D macroporous Ni foams through an electrodeposition method combined with a simple dealloying process. The NPG films supported on Ni foam provide robust protection and efficiently increase its stability in acid media. The as-fabricated NPG/Ni foam hybrid electrode with 3D hierarchical porous structures exhibits excellent electrochemical performance for H₂O₂ electroreduction in acid media in terms of both activity and durability. This type of hybrid 3D electrode with cost-effective fabrication and promising electrochemical performance shows great potential for applications in fuel cell technologies.

Acknowledgments

G.F.C. gratefully acknowledges the financial support by National Natural Science Foundation of China (51271205, 50801070), "The Fundamental Research Funds for the Central Universities" (11lgpy08), "Guangzhou Pearl Technology the Nova Special Project" (2012J2200058), "Research and Application of Key Technologies Oriented the Industrial Development" (90035-3283309), "Plan of Science and Technology Project" by the DaYa Gulf district in Huizhou city (31000-4207387), the Innovative Laboratory Fund by Sun Yat-Sen University and Foundation for Distinguished Young Teachers in Higher Education of Guangdong, China (Yq2013006).

References

- [1] N. Luo, G.H. Miley, K.J. Kim, R. Burton, X.Y. Huang, *J. Power Sources* 185 (2008) 685–690.
- [2] D.X. Cao, D.D. Chen, J. Lan, G.L. Wang, *J. Power Sources* 190 (2009) 346–350.
- [3] L.H. Yi, B.A. Hu, Y.F. Song, X.Y. Wang, G.S. Zou, W. Yi, *J. Power Sources* 196 (2011) 9924–9930.
- [4] S.J. Lao, H.Y. Qin, L.Q. Ye, B.H. Liu, Z.P. Li, *J. Power Sources* 195 (2010) 4135–4138.
- [5] X.L. Yan, F.H. Meng, Y. Xie, J.G. Liu, Y. Ding, *Sci. Rep.* 2 (2012) 941.
- [6] L.F. Gu, N. Luo, G.H. Miley, *J. Power Sources* 173 (2007) 77–85.
- [7] T. Bewer, T. Beckmann, H. Dohle, J. Mergel, D. Stoltzen, *J. Power Sources* 125 (2004) 1–9.
- [8] F. Yang, K. Cheng, Y.H. Mo, L.Q. Yu, J.L. Yin, G.L. Wang, D.X. Cao, *J. Power Sources* 217 (2012) 562–568.
- [9] T.C. Nagaiah, D. Schafer, W. Schuhmann, N. Dimcheva, *Anal. Chem.* 85 (2013) 7897–7903.
- [10] X. Li, D. Heryadi, A.A. Gewirth, *Langmuir* 21 (2005) 9251–9259.
- [11] K. Cheng, F. Yang, G.L. Wang, J.L. Yin, D.X. Cao, *J. Mater. Chem. A* 1 (2013) 1669–1676.
- [12] G.L. Wang, D.X. Cao, C.L. Yin, Y.Y. Gao, J.L. Yin, L. Cheng, *Chem. Mater.* 21 (2009) 5112–5118.
- [13] J.S. Jirkovsky, M. Halasa, D.J. Schiffrin, *Phys. Chem. Chem. Phys.* 12 (2010) 8042–8052.
- [14] D.X. Cao, Y.Y. Gao, G.L. Wang, R.R. Miao, Y. Liu, *Int. J. Hydrogen Energy* 35 (2010) 807–813.
- [15] M.J. Rodriguez-Vazquez, M.C. Blanco, R. Lourido, C. Vazquez-Vazquez, E. Pastor, G.A. Planes, J. Rivas, M.A. Lopez-Quintela, *Langmuir* 24 (2008) 12690–12694.
- [16] F. Yang, K. Cheng, T.H. Wu, Y. Zhang, J.L. Yin, G.L. Wang, D.X. Cao, *RSC Adv.* 3 (2013) 5483–5490.
- [17] J. Erlebacher, M.J. Aziz, A. Karma, N. Dimitrov, K. Sieradzki, *Nature* 410 (2001) 450–453.
- [18] Y. Ding, Y.J. Kim, J. Erlebacher, *Adv. Mater.* 16 (2004) 1897–1900.
- [19] Y. Ding, J. Erlebacher, *J. Am. Chem. Soc.* 125 (2003) 7772–7773.
- [20] T. Fujita, P.F. Guan, K. McKenna, X.Y. Lang, A. Hirata, L. Zhang, T. Tokunaga, S. Arai, Y. Yamamoto, N. Tanaka, Y. Ishikawa, N. Asao, J. Erlebacher, M.W. Chen, *Nat. Mater.* 11 (2012) 775–780.
- [21] A. Wittstock, A. Wichmann, J. Biener, M. Baumer, *Faraday Discuss.* 152 (2011) 87–98.
- [22] C.X. Xu, J.X. Su, X.H. Xu, P.P. Liu, H.J. Zhao, F. Tian, Y. Ding, *J. Am. Chem. Soc.* 129 (2007) 42–43.
- [23] A. Wittstock, V. Zielasek, J. Biener, C.M. Friend, M. Baumer, *Science* 327 (2010) 319–322.
- [24] S. Tanaka, T. Minato, E. Ito, M. Hara, Y. Kim, Y. Yamamoto, N. Asao, *Chem. Eur. J.* 19 (2013) 11832–11836.
- [25] L.H. Qian, X.Q. Yan, T. Fujita, A. Inoue, M.W. Chen, *Appl. Phys. Lett.* 90 (2007) 153120.
- [26] X.Y. Lang, L.Y. Chen, P.F. Guan, T. Fujita, M.W. Chen, *Appl. Phys. Lett.* 94 (2009) 213109.
- [27] X.Y. Lang, A. Hirata, T. Fujita, M.W. Chen, *Nat. Nanotechnol.* 6 (2011) 232–236.
- [28] L.Y. Chen, Y. Hou, J.L. Kang, A. Hirata, T. Fujita, M.W. Chen, *Adv. Energy Mater.* 3 (2013) 851–856.
- [29] E. Detsi, P. Onck, J.T.M. De Hosson, *ACS Nano* 7 (2013) 4299–4306.
- [30] X.Y. Lang, H.Y. Fu, C. Hou, G.F. Han, P. Yang, Y.B. Liu, Q. Jiang, *Nat. Commun.* 4 (2013) 2169.
- [31] R. Zeis, T. Lei, K. Sieradzki, J. Snyder, J. Erlebacher, *J. Catal.* 253 (2008) 132–138.
- [32] N.A. Jarrah, F.H. Li, J.G. van Ommen, L. Lefferts, *J. Mater. Chem.* 15 (2005) 1946–1953.
- [33] W.J. Zhou, X.J. Wu, X.H. Cao, X. Huang, C.L. Tan, J. Tian, H. Liu, J.Y. Wang, H. Zhang, *Energy Environ. Sci.* 6 (2013) 2921–2924.
- [34] Y.H. Chang, C.T. Lin, T.Y. Chen, C.L. Hsu, Y.H. Lee, W.J. Zhang, K.H. Wei, L.J. Li, *Adv. Mater.* 25 (2013) 756–760.
- [35] D.X. Cao, L.M. Sun, G.L. Wang, Y.Z. Lv, M.L. Zhang, *J. Electroanal. Chem.* 621 (2008) 31–37.
- [36] S. Trasatti, O.A. Petrii, *Pure Appl. Chem.* 63 (1991) 711–734.
- [37] F. Yang, K. Cheng, T.H. Wu, Y. Zhang, J.L. Yin, G.L. Wang, D.X. Cao, *J. Power Sources* 233 (2013) 252–258.
- [38] K. Cheng, F. Yang, Y. Xu, L. Cheng, Y.Y. Bao, D.X. Cao, G.L. Wang, *J. Power Sources* 240 (2013) 442–447.